Fluid modelling of an atmospheric pressure dielectric barrier discharge in cylindrical geometry

IOP PUBLISHING JOURNAL OF PHYSICS D: APPLIED PHYSICS

J. Phys. D: Appl. Phys. **42** (2009) 205206 (12pp) doi:10.1088/0022-3727/42/20/205206

Fluid modelling of an atmospheric pressure dielectric barrier discharge in cylindrical geometry

D Petrović[1,2], T Martens[1], J van Dijk[3], W J M Brok[3] and A Bogaerts[1]

[1] Research group PLASMANT, Department of Chemistry, University of Antwerp, Belgium
[2] Institute of Physics, University of Belgrade, Serbia
[3] Department of Applied Physics, Eindhoven University of Technology, The Netherlands

E-mail: dragana.petrovic@ua.ac.be

Received 5 June 2009, in final form 1 September 2009
Published 24 September 2009
Online at stacks.iop.org/JPhysD/42/205206

Abstract

A numerical parameter study has been performed for a cylindrical atmospheric pressure dielectric barrier discharge (DBD) in helium with nitrogen impurities using a two-dimensional time-dependent fluid model. The calculated electric currents and gap voltages as a function of time for a given applied potential are presented, as well as the number densities of the various plasma species. This study shows that for the geometry under consideration the applied voltage parameters have a large impact on the electric current profiles and that the discharge current is always determined by the electron and ion conduction currents while the displacement current is nearly negligible. A relative broadening of the current profiles (compared with the duration of the half cycle of the applied voltage) with an increase in the applied frequency is obtained. Nearly sinusoidal current wave forms, usually typical for radio frequency DBDs, are observed while still operating at the frequencies of tens of kilohertz. For the setup under investigation, the Townsend mode of the DBD is observed in the entire range of applied voltage amplitudes and frequencies. It is shown that the average power density dissipated in the discharge increases with rising applied voltage and frequency. An increase in applied voltage frequency leads to an increase in the electron density and a decrease in electron energy, while increasing the voltage amplitude has the opposite effect.

(Some figures in this article are in colour only in the electronic version)

1. Introduction

Due to their non-thermal character, dielectric barrier discharges (DBDs) have long been applied as chemical reactors for thermodynamically unfavourable chemistries such as the production of ozone [1]. Indeed, DBDs operate at room temperature while the electrons are highly energetic. These highly energetic electrons will lead to the generation of some highly active species including radicals, which is very desirable for the purpose of a chemical reactor for organic gas conversion applications [2]. In this way, some chemical reactions that thermodynamically would not occur at such low gas temperatures are enabled in DBDs, making them efficient plasma-chemical reactors. However, to obtain the best possible results from plasma conversion, the discharge parameters should be well controlled.

Our aim is to develop a model for a DBD used as a chemical reactor for the conversion of greenhouse gases into value added chemicals in an economically efficient way. Energy cost is one of the most important issues that affect such practical applications. Plasma diagnostics are very important in order to understand the detailed chemistry and energy dissipation in the discharge, but for the small dimensions encountered in these kinds of DBDs, numerical simulations are a necessary diagnostic tool. As a first step in determining the optimum operating conditions, we have studied the influence of the applied voltage parameters on the discharge characteristics.

Various DBD designs are used for experimental investigations and industrial applications. DBDs with cylindrically shaped electrodes are more appropriate for applications such as gas conversion than DBDs with planar electrodes and such plasma-chemical reactors are already used

by several research groups [3–10]. In the literature, however, mostly the diagnostics of DBDs in a planar configuration are reported [11–13], while studies of electrical characteristics of DBDs in a cylindrical geometry are rare [14, 15].

In order to obtain a better understanding of the influence of basic operational parameters such as the applied voltage amplitude and frequency, we present and compare in this paper the spatial and temporal distributions of the different formed species in the plasma. At the frequencies of several tens of kilohertz, a permanent presence of excited species in the discharge has been observed. Consequently, Penning ionization constantly provides for the charged particles in the discharge gap, which can explain the radio frequency like behaviour of the electric current profiles at these frequencies. Indeed, the calculated current wave forms show an unconventional sine shape behaviour, which is characteristic for atmospheric radio frequency DBDs [16], at several tens of kilohertz. A small asymmetry of the species density profiles for two successive half periods can also be noticed due to the asymmetry of the reactor electrodes, i.e. due to the difference in their surface areas. In addition, we analyse the total electric current and its current components and analyse the power that is dissipated in the discharge for different combinations of voltage amplitude and frequency.

The paper is organized as follows: in section 2 the numerical model and the basic equations are given. A short description of the setup under consideration and the operating conditions can be found in section 3. In section 4 the results obtained with the numerical model are presented and discussed. Section 5 contains the summary and final conclusions.

2. Numerical model

For all results reported in this paper, a two-dimensional time-dependent fluid model which is part of the Plasimo program [17] has been applied. It was originally developed by Hagelaar for a DBD used in plasma display panels [18] and later transformed and extended by Brok and van Dijk and integrated into the Plasimo program [19, 20].

2.1. Basic equations

The model is based on the continuity equations and equations of motion (in drift–diffusion approximation) for each type of particles treated:

$$\frac{\partial n_\alpha}{\partial t} + \vec{\nabla}\cdot\vec{\Gamma}_\alpha = S_\alpha, \qquad S_\alpha = \sum_j c_{\alpha j} R_{\alpha j}, \tag{1}$$

$$\vec{\Gamma}_\alpha = \pm\mu_\alpha \vec{E} n_\alpha - D_\alpha \vec{\nabla} n_\alpha, \tag{2}$$

where n_α, $\vec{\Gamma}_\alpha$, μ_α and D_α are the number density, flux, mobility and diffusion coefficient of species α, respectively, and $\vec{E}$ is the electric field. The index α refers to the different species including electrons, various ions and neutral species. The source term S_α accounts for the production and destruction of species α due to chemical reactions, in which $R_{\alpha j}$ is the reaction rate and $c_{\alpha j}$ is the stoichiometric coefficient of species of type α created or lost in the reaction of type j. The reaction rate $R_{\alpha j}$ is determined by the reaction rate coefficient k_j, multiplied with the number densities of the reacting species. For the neutral species, the first term in (2) is zero.

For the electrons an energy-balance equation is also solved:

$$\frac{\partial n_e \bar{\varepsilon}}{\partial t} + \vec{\nabla}\cdot\vec{\Gamma}_{\bar{\varepsilon}} = S_{\bar{\varepsilon}}, \tag{3}$$

where $\bar{\varepsilon}$ is the mean electron energy and $\vec{\Gamma}_{\bar{\varepsilon}}$ is the electron energy flux density given by [21]

$$\vec{\Gamma}_{\bar{\varepsilon}} = -\tfrac{5}{3}\mu_e \vec{E} n_e \bar{\varepsilon} - \tfrac{5}{3} n_e D_e \vec{\nabla}\bar{\varepsilon}. \tag{4}$$

The electron energy source term $S_{\bar{\varepsilon}}$ represents the energy loss due to ionizations, excitations and dissociations and the gain of energy due to superelastic collisions and Ohmic heating under the influence of the electric field. For the ions and neutral species no energy-balance equation needs to be included, because these species can be regarded at the same energy (temperature) as the background gas. Moreover, for these species the local field approximation can be used, i.e. the mobility and diffusion coefficients of the heavy particles are taken to be functions of the local reduced electric field (local field divided by pressure). The used values are taken from [22].

In order to obtain a self-consistent electric field distribution also the Poisson equation is solved:

$$\epsilon\vec{\nabla}\cdot\vec{E} = \sum_\alpha q_\alpha n_\alpha, \tag{5}$$

where ϵ is the permittivity of the medium. Note that the Poisson equation is not only solved within the plasma but also inside the dielectrics, where it is reduced to $\epsilon\vec{\nabla}\cdot\vec{E} = 0$ because no species are present inside the dielectrics.

The effect of charge accumulation on the dielectric materials is also taken into account using Gauss's law:

$$\varepsilon_{\text{dielectric}}\vec{E}_{\text{dielectric}}\cdot\vec{e}_n - \varepsilon_{\text{gas}}\vec{E}_{\text{gas}}\cdot\vec{e}_n = \sigma, \tag{6}$$

where $\vec{E}_{\text{dielectric}}$ and $\vec{E}_{\text{gas}}$ are the electric fields inside the dielectric and in the discharge gas, respectively. $\vec{e}_n$ is the normal unit vector pointing to the wall where the charge accumulation occurs. The charge accumulation is calculated from the charge particle flux directed to the surface and it leads to the surface charge density σ on the dielectric.

2.2. Input data in the model

The model is applied to a DBD in helium at atmospheric pressure with 100 ppm of nitrogen impurity. Trace impurity gases are always present in noble gases containers and because the experimental setups cannot be perfectly airtight, the working discharge gas can be contaminated by the residual air. The exact composition of impurity species in the discharge is usually unknown, but as described in earlier work [29] we use nitrogen as impurity, because it is the main component of air and we use it as a model impurity in order to correctly describe the Penning ionization of molecular impurities on the breakdown of the gas. The impurity level of 100 ppm chosen here is exactly the same as used in [30] on which our physical model and the chemical description previously have been validated. The gas temperature is assumed to be 300 K,

uniformly distributed over the discharge. The species included in the model are the background gas He, the impurity gas N_2, the electrons, the He^+, He_2^+, N_2^+ and N_4^+ ions, the He_2^* excimers and He atoms excited to the metastable levels.

The chemical reaction set contains 18 chemical reactions and it can be found in [29]. Since the nitrogen is considered as an impurity (in the parts per million range), following the example of [30], we assume that its main influence consists in its impact on the ionization kinetics through Penning ionization. In the conditions under consideration in this study, the plasma is highly collisional and consequently excited states of nitrogen are quickly quenched due to a high collision frequency and the importance of the excited states of nitrogen is very limited. Hence, the nitrogen radical and metastable states are neglected in this study, but that may be important at higher nitrogen concentrations.

The electron energy loss associated with the vibrational and rotational excitation of nitrogen gas is included as an energy loss term in the electron energy equation. Excitations of molecular nitrogen to a rotational level of 0.02 eV and to two vibrational levels of 0.29 and 0.291 eV are included as additional energy loss terms in equation (4).

For most of the electron-induced processes the reaction rates are calculated based on energy dependent cross sections, with a separate program, called BOLSIG+, which is based on the two-term expansion of the Boltzmann equation [23]. This program is applied for a wide range of different, fixed reduced electric field values. For each value of the reduced electric field the average electron energy, the mobility of the electrons and the rates of the different electron-induced processes are tabulated. By the use of these tables the rates, mobilities and diffusion coefficients are applied corresponding to the electron energy calculated with (4). The diffusion coefficients are derived from the mobilities using the Einstein relationship, assuming Maxwellian bulk electrons. Details about the chemistry model can be found in [24, 25].

The boundary conditions for the electrons are largely determined by secondary electron emission from the dielectrics due to ion bombardment. Following the procedure of Hagelaar *et al* [26] we use a constant secondary electron emission coefficient of 0.05 for the helium ions and 0.001 for nitrogen ions. Moreover, we assume that this ion-induced secondary electron emission produces electrons with a mean initial energy of 4 eV [27]. Reflection at the walls is neglected and electron desorption from the dielectrics is not considered, because it has been stated [28] that the latter process is very unlikely to happen.

Equations (1)–(5) are solved by means of the control volume method. Consequently, the code is suitable for the description of both Cartesian as well as cylindrical geometries. The nature of the coordinate system is reflected only in the way the geometrical quantities are calculated. Details on the implementation can be found elsewhere [18].

3. Setup and conditions

The model was applied to a cylindrical DBD reactor consisting of two coaxial stainless steel electrodes with a 2 mm thick alumina dielectric on the inner side of the outer electrode, as illustrated in figure 1. The length of the reactor is 9 cm and the outer diameter is 3 cm. The gap width can be varied by changing the diameter of the inner tube. For this study the gap width is kept fixed at 0.7 mm. A sine shaped high voltage is applied on the inner electrode in the frequency range from 0.25 to 100 kHz. The outer electrode is grounded.

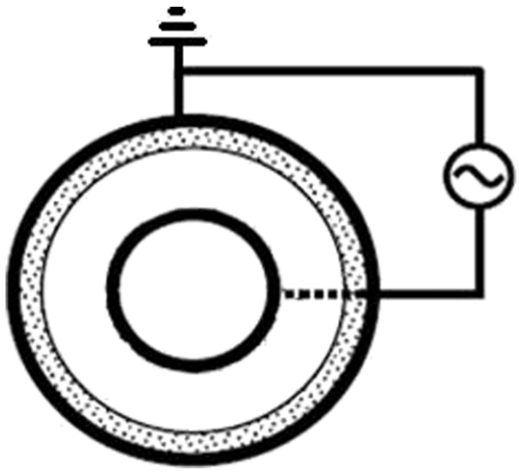

Figure 1. Schematic diagram of the setup used in the simulations. The inner electrode is powered while the outer one is grounded.

The presented geometry is very suitable for plasma assisted gas oxidation and gas conversion. Similar setups are already in use in several experimental groups [4, 8, 9] and are industrially applied for the production of ozone [1].

The physical model and the chemical description have been validated versus experimental data for a DBD with planar electrodes [29]. The setup parameters were chosen to be the same as used by Mangolini and coworkers [30] and very similar to the parameters used by Massines and coworkers [11]. The study has shown that the plasma model is suitable for the simulation of DBDs between two parallel-plane electrodes and that it gives accurate and reliable results.

For validation of the results in the study of a DBD between two coaxial electrodes as presented here, calculations were performed in the comparable parallel electrode configuration, keeping the gap distance and the dielectric thickness the same as in the coaxial setup. The same electrical behaviour and trends and similar temporal profiles of plasma parameters were observed. Taking this into account, we assume that our numerical model can simulate a DBD with cylindrically shaped electrodes with the same accuracy and reliability as a DBD with parallel-plate electrodes.

4. Results and discussion

4.1. Electrical characteristics of the discharge

The calculated spatially averaged total electric current densities as well as the calculated gap voltages are plotted as a function of time in figure 2, for different values of applied voltage at a frequency of 1 kHz. A clear transition from one narrow peak to a multipeak can be seen, when the

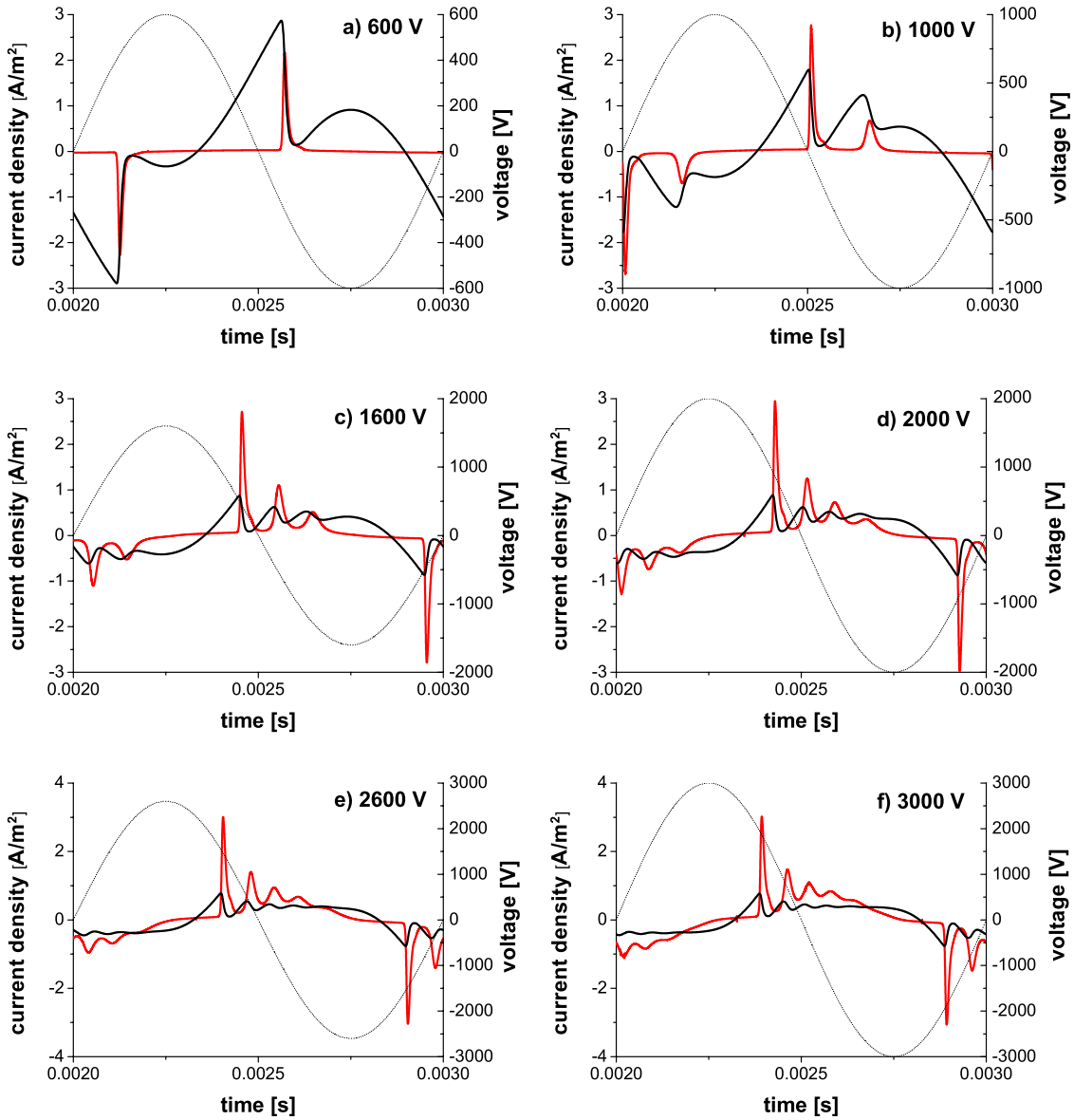

Figure 2. Calculated total current densities (red solid lines) and gap voltages (black solid lines) as a function of time in an atmospheric DBD in helium with 100 ppm nitrogen impurity, for different applied voltages (black dotted lines). The applied frequency is 1 kHz. (Colour online.)

applied voltage amplitude increases. Single narrow peaks as in figure 2(*a*) are usually reported in the literature for helium DBDs [11, 12, 30]. However, a multiple breakdown in the system due to an increase in the applied voltage has also been reported [12, 13, 31]. As can be seen in figure 2(*c*), at the applied voltage of 1.6 kV, three current peaks appear during one half cycle instead of one at 600 V (figure 2(*a*)). The origin of the multi-breakdown is investigated by several authors [12, 13, 31] and it has been shown that the density of accumulated charges on the dielectric increases with the increase in the applied voltage causing the memory voltage to enhance the external voltage. Therefore, when the first current pulse quenches, the gas gap voltage can exceed the breakdown voltage again, and consequently a second current pulse is produced in the same half cycle.

The successive peaks in one multipeak discharge sequence are characterized by a decreasing amplitude and increasing width. There are two possible mechanisms which explain the decreasing behaviour of the amplitude. As has been shown in [12, 31], the memory voltage (due to accumulated charges on the dielectric surfaces) first enforces an electrical field between the electrodes while at the later stage of a multipeak discharge sequence, it weakens this electrical field, thereby decreasing the ionization rate and causing a monotonic diminishing in the amplitude of the current density pulses. In [13], the same phenomenon has been explained by enhanced Penning ionization due to an increased number density of metastables over the first quadrant in each half cycle of the applied voltage.

The absolute value of the main maximum of the current density slightly increases with rising applied voltage amplitude in transition from one to two current peaks and stays more or less the same with the further voltage amplitude increase. However, the total $\int I \, \mathrm{d}t$ increases with rising of applied

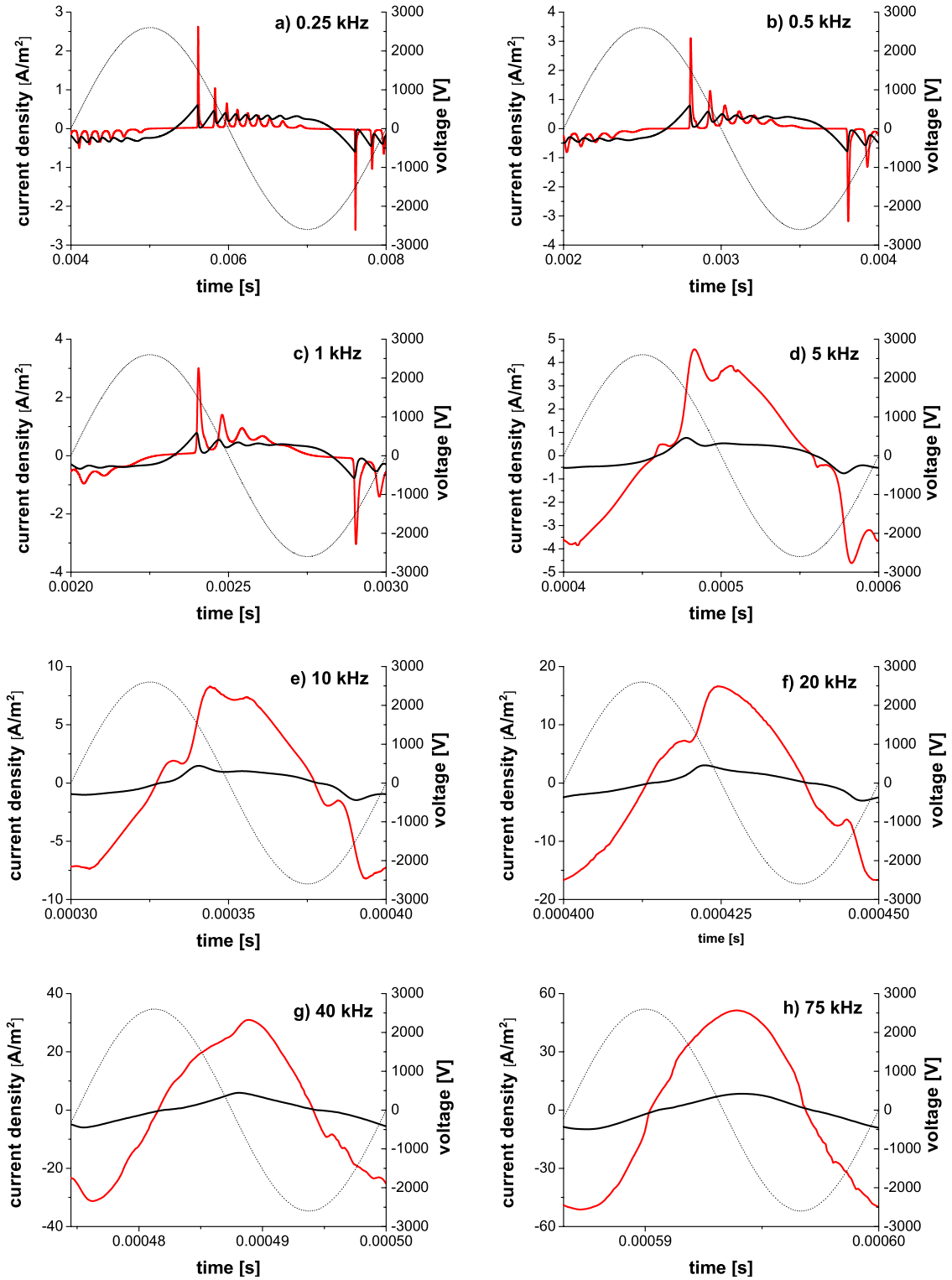

Figure 3. Calculated total current densities (red solid lines) and gap voltages (black solid lines) as a function of time in an atmospheric DBD in helium with 100 ppm nitrogen impurity, for different applied frequencies. The applied voltage is 2.6 kV (black dotted lines). (Colour online.)

voltage due to the appearance of the second, third and the higher order peaks.

An increase in the applied frequency, however, does not go in favour of multipeak appearance as can be seen in figure 3. For an applied voltage of 2.6 kV the multipeak behaviour is very pronounced for low frequencies such as 250 and 500 Hz as shown in figures 3(*a*) and (*b*). An increase in the applied frequency leads to a decrease in the number of current pulses. For applied frequencies of 0.25, 0.5 and 1 kHz the effect is illustrated in figures 3(*a*)–(*c*), respectively. The same trend has been experimentally observed in [13, 32], however, for different DBD setups. At higher frequencies,

starting from 5 kHz, there is no real second breakdown in the system, although some indication for a second current maximum exists. The current density does decrease after reaching the maximum, but it does not go to zero, which indicates that there is no quenching of the discharge between pulses as for the lower applied frequencies. Indeed, at the higher applied frequencies there is not enough time in between pulses for the discharge to relax.

A further increase in the applied frequency causes a complete disappearance of multipeaks and leads to smoothing of the current profile. At the same time, the pulse length increases relative to the period of applied voltage. Indeed, the slope of the external voltage becomes so steep that the breakdown voltage cannot be achieved more than once in the same half cycle. At the highest frequencies investigated (75 kHz, figure 3(*h*)) a nearly sinusoidal current waveform is obtained.

A significant increase in the absolute values of the current density maxima with rising frequency is also apparent from figure 3. This is in good agreement with experimental results [32] where the same trend of the current density was observed, although in a parallel-plate geometry. Note that it was not possible to obtain one narrow current peak at this applied voltage, for any of the frequencies investigated.

A relative broadening of the electrical current profiles (compared with the duration of the half cycle of the applied voltage) with an increase in the applied frequency is even more obvious for an applied voltage of 600 V, which does not cause multi-breakdown in the discharge, as can be seen in figure 4. Indeed, there is a clear transition from a very narrow peak at 1 kHz to a very broad one at 75 kHz. First, note that at frequencies below 1 kHz it was not possible to obtain a sustainable discharge for this applied voltage of 600 V. At the frequency of 1 kHz, the current density profile is characterized by a very narrow current peak, one per half cycle. An increase in the applied frequency to 2 kHz causes relative broadening of the current peak (see figure 4(*b*)) and this trend is even more obvious for the frequency of 5 kHz, as can be seen in figure 4(*c*). A further increase in the applied frequencies continues to broaden the current peaks, although some oscillations in amplitude and some local maxima can also be noticed (figures 4(*d*)–(*e*)).

Although the current peaks are relatively broad compared with the applied voltage periods, the rise time and absolute width of the current peaks decrease with the increase in the frequency, which is in good agreement with the experiment [13]. Indeed, looking at the absolute values of the time in the x-axis, the electric current pulse duration decreases from the order of 10^{-5} s at the applied frequency of 1 kHz to the order of 10^{-6} s at 100 kHz. Finally, the absolute values of the current density maxima increase with rising frequency, as is clear from figure 4. However that increase is not so pronounced as in the case of the higher applied voltage (figure 3).

The black solid lines in figures 2, 3 and 4 represent the calculated gap voltages. The discharge occurs when the gap voltage reaches the breakdown voltage and results in significant electron production. For the lower applied frequencies (approximately up to 2 kHz) the gap voltage decreases as soon as a single or multiple breakdown occurs, due to the charging of the dielectric barriers [33]. For higher frequencies a different mechanism occurs. Figures 3(*d*)–(*h*) demonstrate that the gap voltage continues to increase after the breakdown. For these frequencies the charged particles do not get enough time to charge the dielectrics, so the gap voltage does not become adequately quenched before the electrode polarity changes. Moreover, this appears to give rise to a pre-breakdown effect which can be seen in figures 4(*d*)–(*f*).

4.2. Discharge mode

It is known that atmospheric pressure DBDs can operate in two discharges modes, i.e. glow mode and Townsend mode, characterized by different electrical characteristics. Figures 2, 3 and 4 suggest that the discharge is in Townsend mode, because it is usually associated with current densities in the order of a few A m^{-2} till tens of A m^{-2}. This is as expected [12], because in the setup under consideration the dielectric barrier is thick compared with the gap width, i.e. 2 mm versus 0.7 mm.

The type of discharge mode is reflected in the spatial profiles of the electric field and the species densities. As an illustration, two examples of the calculated spatial distribution of electron and total ion densities together with the electric field distribution in the radial direction (i.e. over the gas gap) at the moment of the current density maximum are shown in figure 5. Similar profiles are observed for the entire range of the applied voltage and frequency. The charge density has no strong influence on the electric field and there is a clear absence of a cathode fall region.

There is no quasineutral plasma region and the ion and electron densities differ from two orders of magnitude at lower applied frequency to one order of magnitude at higher frequencies (see figure 5). Note that at the highest frequencies investigated, the current density is high enough to indicate the onset of the glow regime. Indeed, at the maximum current density, the maximum ion density is in the order of 10^{17} m^{-3}, which is enough for the cathode fall formation. However, the spatial structure of the electric field indicates that the discharge is still in Townsend mode or in a so-called sub-normal glow mode [35] because it is not constant over the discharge gap, but it is rising almost linearly.

4.3. Electric current components and dissipated power

The total electric current, I_{tot}, measured in the experiments is the sum of the discharge current, I_{disch}, and the external circuit capacitive displacement current, $I_{\mathrm{ext,dis}}$. The discharge current, which characterizes the discharge behaviour, consists of a conduction part, I_{cond} (due to the flow of electric charges) and a displacement part (due to the capacitive nature of the gas gap) which can be expressed as

$$I_{\mathrm{tot}} = I_{\mathrm{disch}} + I_{\mathrm{ext,dis}}, \tag{7}$$

$$I_{\mathrm{disch}} = -I_{\mathrm{ion}} + I_{\mathrm{e}} + I_{\mathrm{dis}}. \tag{8}$$

The first term in (8) is the ion current. It is chosen to be negative, corresponding to a flow of positive ions from the

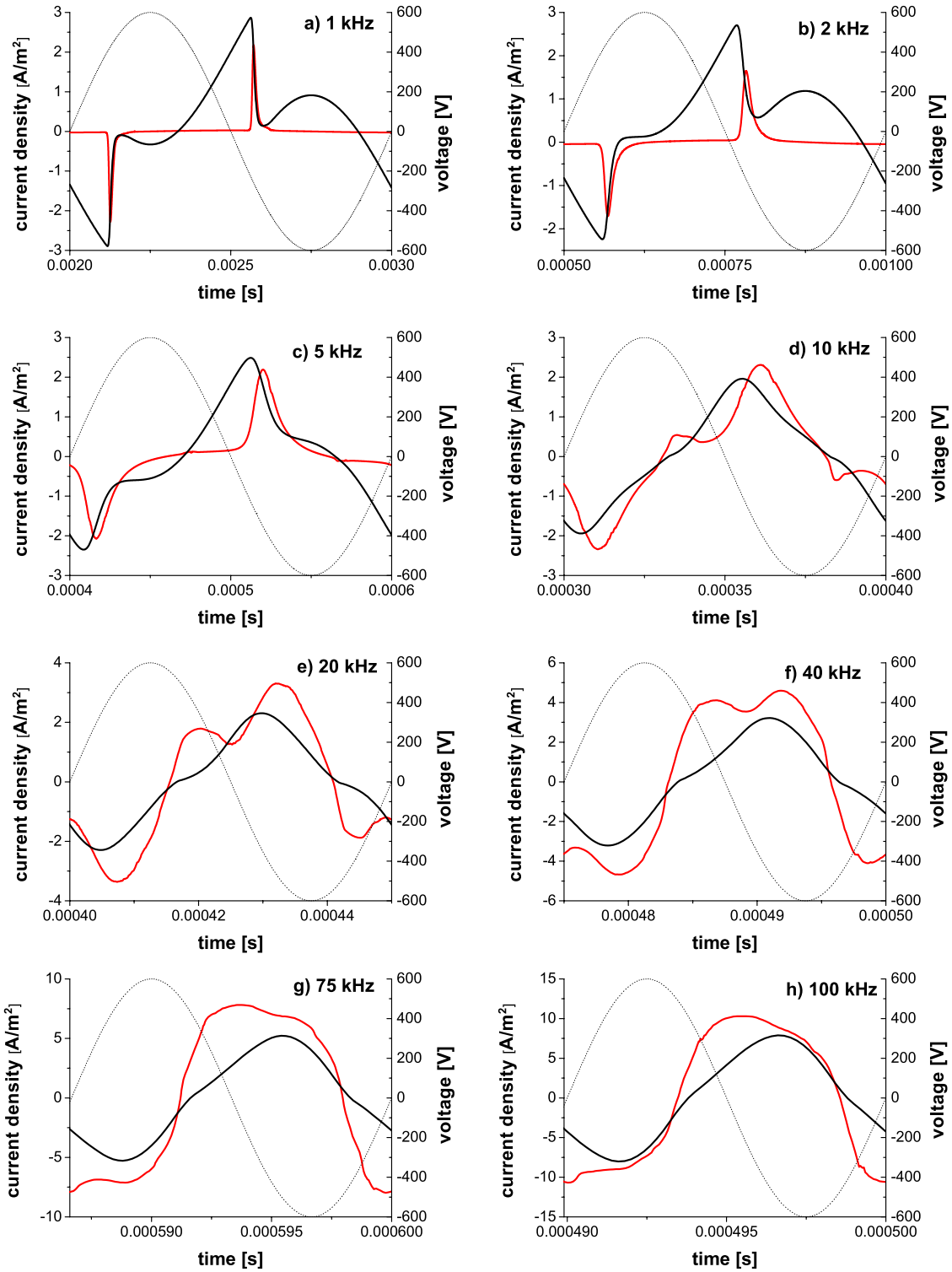

Figure 4. Calculated total current densities (red solid lines) and gap voltages (black solid lines) as a function of time in an atmospheric DBD in helium with 100 ppm nitrogen impurity, for different applied voltages (black dotted lines). The applied voltage amplitude is 0.6 kV. (Colour online.)

plasma to the electrode. The total ion current is the sum of the fluxes of each ionic species, weighted by their charge. In this case, all ionic species are singly charged, so the total ion current is closely related to the total ion flux. The second term is the electron current and the third term is the gas displacement current. The displacement current arises because the surface charge Q varies as a function of time during the applied voltage cycle, causing a current $\mathrm{d}Q/\mathrm{d}t$ to flow in the electrical connections of the electrodes.

For the purpose of studying the energy efficiency of the plasma-chemical reactor it is important to distinguish between these current components. The power dissipated in the system,

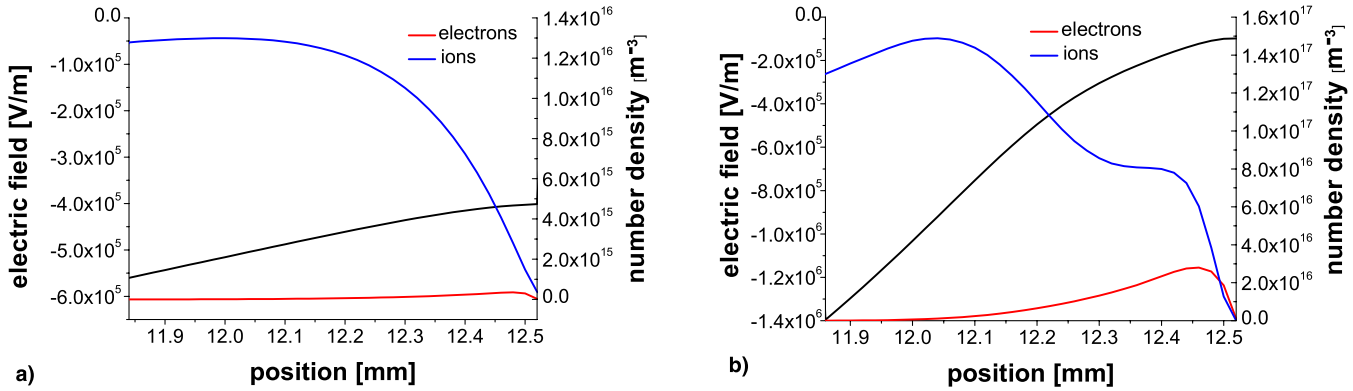

Figure 5. Calculated spatial number density profiles of electrons and sum of all ions (right axes) and spatial electric field distribution (left axes) in the radial direction (i.e. over the gas gap) at the maximum current densities for the applied voltage frequencies and amplitudes of (*a*) 2 kHz and 0.6 kV and (*b*) 75 kHz, 2.6 kV. The powered electrode is at the left-hand side and currently at a negative potential. The space filled with dielectric is not shown.

Table 1. Calculated spatially and time averaged dissipated power density and electron energy and density at the applied voltage of 2.6 kV, for different applied frequencies.

Applied frequency (kHz)	Power density (W cm^{-3})	Electron energy (eV)	Electron density (m^{-3})
0.5	0.084	6.05	10^{13}
5	0.919	5.98	10^{14}
10	1.823	5.49	10^{15}
20	3.582	4.73	10^{16}
75	15.641	4.55	10^{17}

Table 2. Calculated spatially and time averaged dissipated power density and electron energy and density at the applied frequency of 1 kHz for different applied voltages.

Applied voltage (V)	Power density (W cm^{-3})	Electron energy (eV)	Electron density (m^{-3})
0.6	0.031	4.29	8.29×10^{13}
1	0.054	5.08	6.28×10^{13}
1.6	0.091	5.79	3.29×10^{13}
2	0.124	5.88	2.68×10^{13}

P_{diss}, is the product of the conduction current and gap voltage:

$$P_{\mathrm{diss}}(t) = V_{\mathrm{gap}}(t) I_{\mathrm{cond}}(t), \tag{9}$$

while the supplied power, P_{sup}, is the product of the total current and applied voltage, $P_{\mathrm{sup}}(t) = V_{\mathrm{app}}(t) I_{\mathrm{tot}}(t)$.

The average power density consumed in the discharge, calculated as

$$\langle P_{\mathrm{diss}} \rangle = \frac{1}{T} \int_0^T P_{\mathrm{diss}}(t)\, \mathrm{d}t, \tag{10}$$

is found to increase with rising frequency of the applied voltage. As can be seen in table 1, at an applied voltage of 2.6 kV, the dissipated power density is 0.08 W cm^{-3} for a frequency of 0.5 kHz, increasing to 3.58 W cm^{-3} at 20 kHz, up to 15.35 W cm^{-3} at an applied frequency of 75 kHz. As a result of this higher power consumption the electron number density increases from about 10^{13} m^{-3} at the lowest frequency investigated up to an order of 10^{17} m^{-3} at the highest frequency investigated. However, the spatially and time averaged electron energy slightly decreases from 6.05 eV at 0.5 kHz to 4.55 eV at 75 kHz.

On the other hand, for a given applied frequency of 1 kHz, the average electron energy increases with rising voltage, as illustrated in table 2, while their density slightly decreases, but it stays in the same order of magnitude. Furthermore, an increase in the applied voltage amplitude causes a higher dissipated power density as well.

The external circuit is not included in our model and the calculated total current is actually the discharge current. Figure 6 shows, as an illustration, the contributions of the calculated ion and electron conduction currents and of the displacement current to the total discharge current for some applied voltages. The displacement current appears to be negligible for the entire range of frequencies applied. Hence, the relative broadening of the current profiles, which was observed in figures 3 and 4 above, can here not be explained by an increase in the displacement current at rising applied frequency. For example, in [36] a significant contribution of the sinusoidal capacitative current to the total current was reported. In that case, the relatively broad current pulses and transition to a sinusoidal current wave form was attributed to a superposition of the displacement current (sine shaped profiles) and the discharge current (narrow peaks).

Finally, figure 6 illustrates that the electron and ion conduction currents participate equally in the discharge current. The electron current is zero during the first, rising half cycle. Therefore, the value of the discharge current in that half cycle is more or less equal to the ion current and vice versa during the second, falling half cycle.

4.4. Plasma species densities

Figures 7(*a*) and (*b*) illustrate the calculated spatially averaged number densities of different plasma species as a function of time, for two different applied voltage amplitudes (0.6 and 2.6 kV), at the frequency of 2 kHz. All species densities have similar temporal profiles and reach their maximum values almost at the same time. However, there is a small delay of the electron and N_4^+ ion maxima compared with the other species.

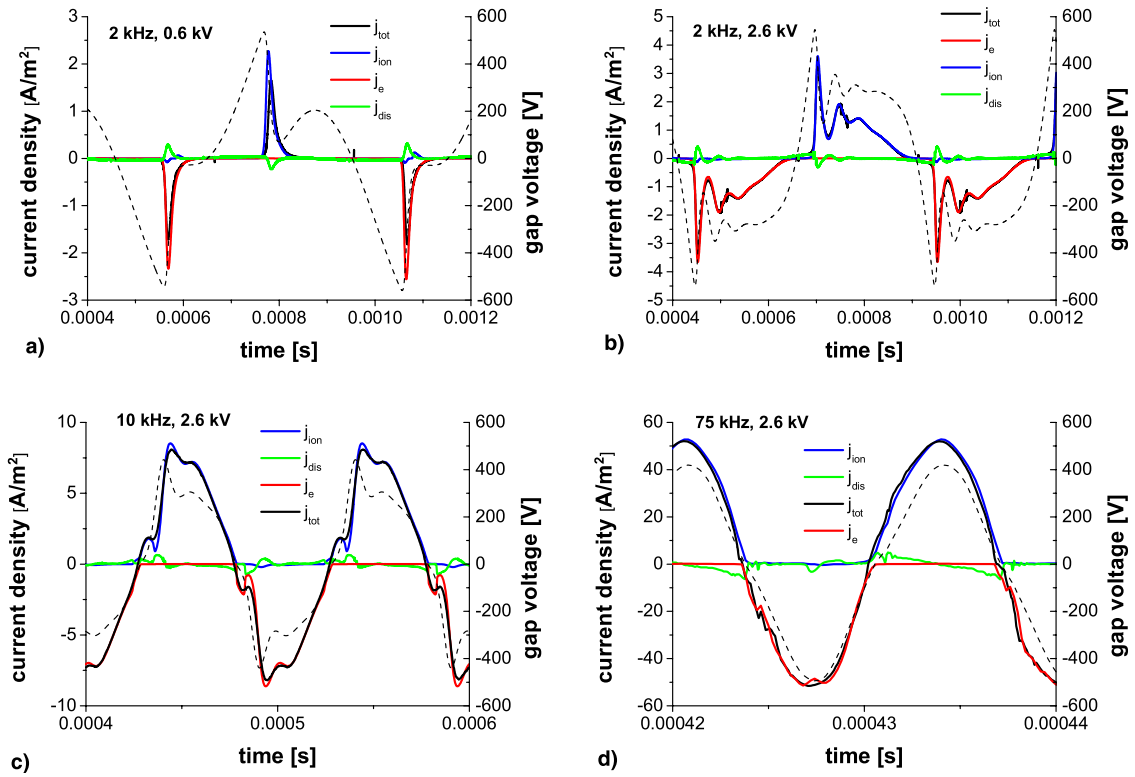

Figure 6. Calculated current density components as a function of time for different applied voltage frequencies and amplitudes. Red and blue lines represent electron and ion conduction current, respectively, and green lines represent displacement current. The black dotted lines represent the gap voltage for the given applied voltage. (Colour online.)

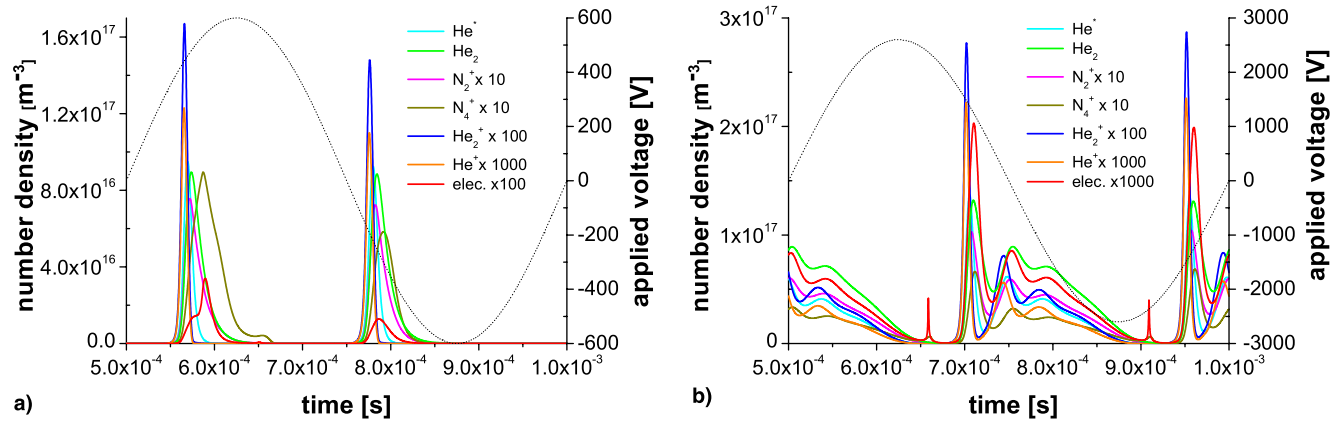

Figure 7. Calculated spatially averaged number densities as a function of time for applied voltage frequencies and amplitudes: (*a*) 2 kHz and 0.6 kV; (*b*) 2 kHz and 2.6 kV (black dotted lines).

The pulsed character of the DBD is clearly reflected in the temporal evolution of the species densities, for both the single pulse as for the multipulse discharge.

Although nitrogen is present only as 100 ppm of impurity, the N_2^+ ions are the most important positive ions, followed by the N_4^+ ions, which are a factor of two lower. Hence, the positive charge in the discharge is completely determined by nitrogen ions whereas helium ions are of minor importance. This effect has been studied in detail by Martens and coworkers in [29]. The maximum density of the He_2^+ ions is one order of magnitude lower than the N_2^+ and N_4^+ ion densities and the He^+ ion density is even negligible compared with them. At the higher frequencies the dominant role of the nitrogen ions remains, as can be seen in figures 8(*a*1) and (*b*1). However, the N_4^+ ions are now the dominant ions, with a density slightly above the N_2^+ ion density. Hence, the electrical characteristics are clearly determined by the nitrogen ions.

It is known that an increase in pressure enforces the role of trace impurities [34]. Indeed, impurities do not affect the dynamics and structure of low-pressure DBDs, but they play a significant role at atmospheric pressure. It is possible that their role is more pronounced at higher frequencies of applied voltage and determine even more the behaviour of a DBD continuously alternating glow and afterglow. This will need to be studied in more detail.

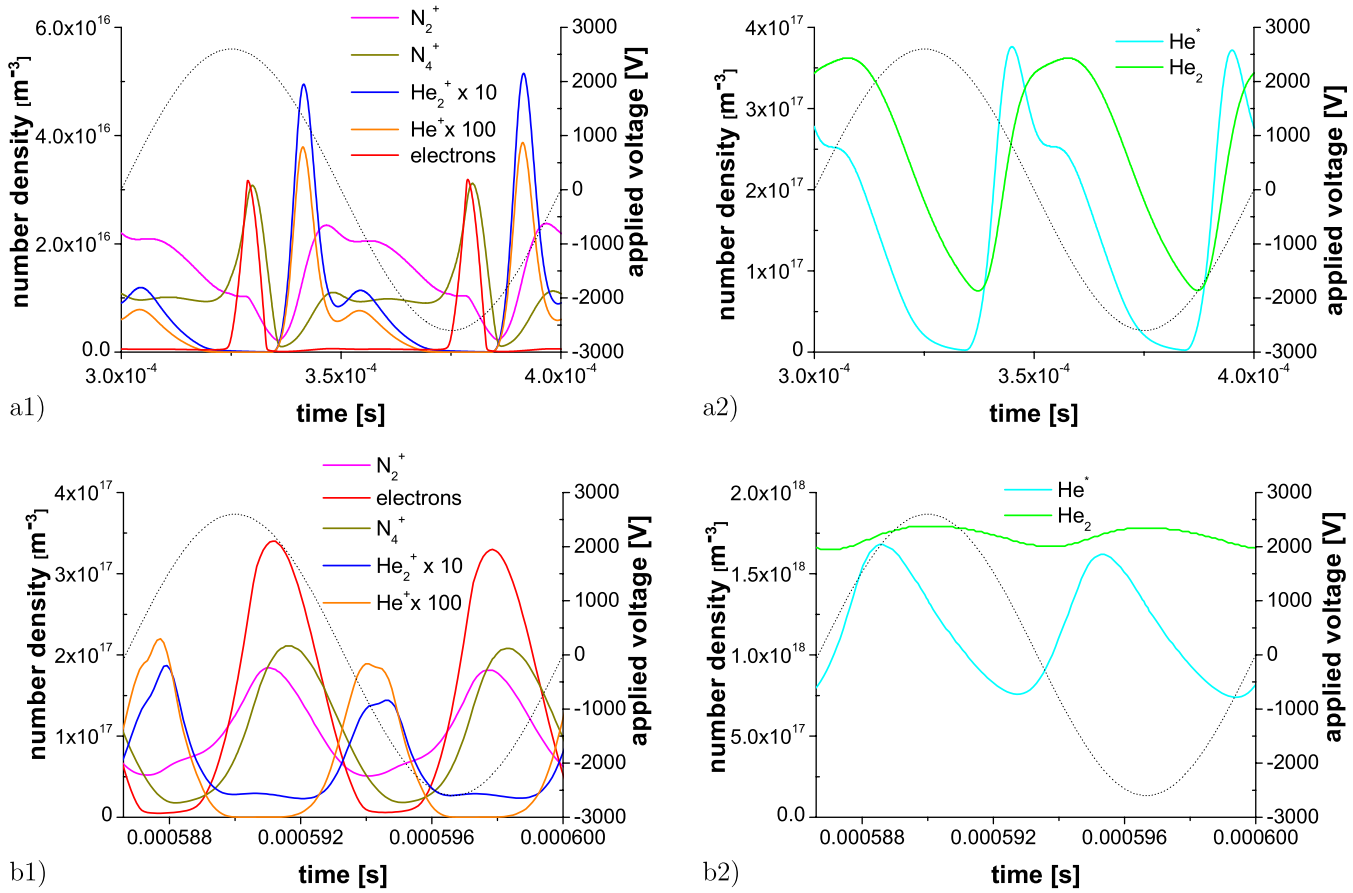

Figure 8. Calculated spatially averaged number densities as a function of time for applied voltage frequencies and amplitudes: (*a*) 10 kHz, 2.6 kV; (*b*) 75 kHz, 2.6 kV (black dotted lines).

As shown in figure 7, the electron densities are about two orders of magnitude lower than the dominant ion densities for the entire range of applied voltages and frequencies investigated. Their density, however, slightly increases at higher frequencies, but still remains one order of magnitude lower, making the bulk positively charged.

An increase in the applied voltage frequency disorganizes the synchronic behaviour of the species densities. The maximum values of species densities are shifted in time, as shown in figure 8. For the sake of clarity, the density profiles of the charged and neutral species are plotted in separate figures. At the frequency of 10 kHz (see figures 8(*a*1) and (*a*2)) all densities still follow the applied voltage pulses and have periodic behaviour. The same is true for the applied voltage frequency of 75 kHz. However, the temporal profiles of the metastables at these higher frequencies differ from those of the charged particles. It can be seen that the density of the metastable helium atoms keeps a relatively high value throughout the entire discharge.

Indeed, the metastable species have a longer lifetime than the charged plasma species, which indicates that there is less quenching of the metastables at the surface. This effect is due to the plasma sheath formation, which creates an accumulation of positively charged species near the dielectric surfaces and consequently an increased positive ion loss at the walls.

The presence of metastable species is crucial in the maintenance of a Townsend discharge. As demonstrated in figure 5, there is no quasineutral bulk in such a discharge, which makes charge trapping in the bulk more difficult [35]. A reasonable minimum of metastable densities is necessary to sustain the presence of charge carriers in the discharge through Penning ionization.

The densities of metastable species at the higher frequencies do not vary a lot with time, which indicates that the gas remains excited all the time. As can be seen in figure 8(*b*2), at the frequency of 75 kHz, the He_2^* excimer number density is almost constant in time. It is also the highest density in the discharge in the order of 10^{18} m^{-3}. This high production of metastables and thus higher Penning ionization of the nitrogen can be a possible explanation for a longer current pulse duration in one half cycle of the applied voltage.

A small asymmetry of the species density profiles for two successive half periods can also be noticed due to the asymmetry of the reactor electrodes, i.e. due to the difference in their surface areas. However, the difference is not very pronounced because of the small gap distance. Indeed, taking into account that the gap width is 0.7 mm, the active surface of the inner and outer electrodes differs for about 5.6%, which is not enough to have a significant influence on the plasma profiles.

5. Summary and conclusions

We have presented the influence of applied voltage parameters on the discharge characteristics of a cylindrical DBD in helium with nitrogen impurities. The discharge properties of a DBD in cylindrical geometry have not yet been subject to such extensive study as for the parallel-plate configuration, so a direct comparison with experiment is more difficult. However, we have tried to compare our results as much as possible with experimental data from the literature.

This study shows that the applied discharge voltage and frequency have a large impact on the electric current profiles, which can range from one narrow peak over multipeak to a sine shaped profile. An increase in the applied voltage can cause multiple breakdowns in the system which is visible in the current profiles as a multipeak behaviour.

An increase in the applied voltage frequency reduces the number of discharge current pulses per half cycle. At the frequencies of tens kilohertz, a single but relatively broad peak behaviour is obtained. A sinusoidal shape of current profiles, usually typical for radio frequency DBDs [16], is observed in the kilokertz range that is different from the conventional pulse-like current waveforms of atmospheric pressure DBDs at these frequencies. For the entire range of voltage amplitudes and frequencies applied, the discharge current is determined mainly by the electron and ion conduction currents while the displacement current is nearly negligible. Hence, the relative broadening of the current profiles here cannot be explained by an increase in the displacement current at rising applied frequency as in some other cases [36] where a significant contribution of the sinusoidal capacitative current to the total current was reported. In the geometry under consideration in this work, a permanent presence of excited species in the discharge has been observed at the frequencies of several tens of kilohertz. Consequently, the charged particles are constantly produced in the discharge gap that can explain radio frequency like behaviour of the electric current profiles.

At the lower frequencies the number densities of all species reach their maximum values at the same time. However, when applying higher frequencies this regular behaviour is distorted. Although nitrogen is present only as a trace impurity, the electrical characteristics of the discharge are determined by the nitrogen ions for the entire range of frequencies applied, while helium ions are of minor importance. Moreover, at the higher frequencies, some discharge features resemble very much the characteristics of a nitrogen discharge (i.e. longer duration of the current pulse compared with the duration of one half cycle of applied voltage as well as gap voltage behaviour).

For the setup under investigation, low values of the calculated current densities are obtained in the entire range of applied voltage amplitudes and frequencies. This indicates that the discharge is in Townsend mode, which has also been confirmed by the calculated spatial profiles of the electric field and charged species densities, where a clear absence of the cathode fall is observed. It is shown that the average power density dissipated in the discharge increases with rising applied voltage and frequency. The average electron number densities increase with applied voltage frequency, while the average energy of the electrons decreases. Increasing the voltage amplitude has the reciprocal effect.

Acknowledgments

These results were obtained in the framework of the IWT SBO project No 18/2821. Also the CalcUA computing facilities of the University of Antwerp are acknowledged.

References

[1] Kogelschatz U, Eliasson B and Egli W 1999 *Pure Appl. Chem.* **71** 1819
[2] Kogelschatz U 2003 *Plasma Chem. Plasma Process.* **23** 1
[3] Zhou L M, Xue B, Kogelschatz U and Eliasson B 1998 *Plasma Chem. Plasma Process.* **18** 375
[4] Jian T, Li Y, Liu Ch, Xu G, Eliasson B and Xue B 2002 *Catal. Today* **72** 229
[5] Okazaki K, Kishida T, Ogawa K and Nozaki T 2002 *Energy Convers. Manage.* **43** 1459
[6] Zhang Y, Li Y, Wang Y, Liu C and Eliasson B 2003 *Fuel Process. Technol.* **83** 103
[7] Aghamir F M, Matin S N, Jalili A H, Esfarayeni M H, Khodagholi M A and Ahmadi R 2004 *Plasma Sources Sci. Technol.* **13** 707
[8] Pietruszka B, Anklam K and Heintze M 2004 *Appl. Catal. A: Gen.* **261** 984
[9] Song H K, Choi J W, Yue S H, Lee H and Na B K 2004 *Catal. Today* **89** 27
[10] Kim H H, Ogata A and Futamura S 2006 *IEEE Trans. Plasma Sci.* **34** 984
[11] Massines F, Rabehi A, Decomps P and Gardi R B 1998 *J. Appl. Phys.* **83** 2950
[12] Golubovskii Yu B, Maiorov V A, Behnke J and Behnke V G 2003 *J. Phys. D: Appl. Phys.* **36** 39
[13] Radu I, Bartnikas R and Wertheimer M R 2003 *IEEE Trans. Plasma Sci.* **31** 1363
[14] Li X, Zhao N, Fang T, Liu Z, Li L and Dong L 2008 *Plasma Sources Sci. Technol.* **17** 015017
[15] Pal U N *et al* 2009 *J. Phys. D: Appl. Phys.* **42** 045213
[16] Shi J J, Liu D W and Kong M G 2006 *Appl. Phys. Lett.* **89** 081502
[17] http://plasimo.phys.tue.nl
[18] Hagelaar G 2000 Modeling of microdischarges for display technology *PhD Thesis* Department of Applied Physics, Eindhoven University of Technology
[19] Brok W J M, Van Dijk J, Bowden M D, Van der Mullen J J A M and Kroesen G M W 2003 *J. Phys. D: Appl. Phys.* **36** 1967
[20] Brok W J M, Gendre M F and Van der Mullen J J A M 2006 *J. Phys. D: Appl. Phys.* **40** 156
[21] Raizer Y P 1991 *Gas Discharge Physics* (Berlin: Springer)
[22] Ellis H W, Pai R Y and McDaniel E W 1976 *At. Data Nucl. Data Tables* **17** 177
[23] Hagelaar G J M and Pitchford L C 2005 *Plasma Sources Sci. Technol.* **14** 722
[24] Martens T, Bogaerts A, Brok W J M and Van der Mullen J J A M 2005 *J. Anal. At. Spectrom.* **22** 1033
[25] Martens T, Bogaerts A, Brok W J M and Van Dijk J 2007 *Anal. Bioanal. Chem.* **388** 1583
[26] Hagelaar G J M, Kroesen G M W, Slooten U and Schreuders H 2000 *J. Appl. Phys.* **88** 2252
[27] Hagstrum H D 1956 *Phys. Rev.* **104** 1516
[28] Raizer Y P, Shneider M N and Yatsenko N A 1995 *Radio-frequency Capacitive Discharges* (Boca Raton, FL: CRC Press) pp 30–1

[29] Martens T, Bogaerts A, Brok W J M and Van Dijk J 2008 *Appl. Phys. Lett.* **92** 041504
[30] Mangolini L, Anderson C, Heberlein J and Kortshagen U 2004 *J. Phys. D: Appl. Phys.* **37** 1021
[31] Zhang Y, Gu B, Peng X, Wang D and Wang W 2008 *Thin Solid Films* **516** 7547
[32] Shin J and Raja L L 2003 *J. Appl. Phys.* **94** 7408
[33] Brauer I, Punset C, Purwins H-G and Boef J P 1999 *J. Appl. Phys.* **85** 7569
[34] Yuan Y and Raja L 2002 *Appl. Phys. Lett.* **81** 814
[35] Massines F, Ségur P, Gherardi N, Khamphan C and Ricard A 2003 *Surf. Coat. Technol.* **174** 8
[36] Trunec D, Navratil Z, Stahel P, Zajickova L, Bursikova V and Cech J 2004 *J. Phys. D: Appl. Phys.* **37** 2112